ELSEVIER

Journal of Membrane Science 184 (2001) 245–255

journal of MEMBRANE SCIENCE

www.elsevier.nl/locate/memsci

Modeling permeation through anisotropic zeolite membranes with nanoscopic defects

Peter H. Nelson [a], Michael Tsapatsis [b], Scott M. Auerbach [a,b,*]

[a] *Department of Chemistry, University of Massachusetts, Amherst, MA 01003, USA*
[b] *Department of Chemical Engineering, University of Massachusetts, Amherst, MA 01003, USA*

Received 2 August 2000; received in revised form 29 September 2000; accepted 19 October 2000

Abstract

We have modeled permeation through anisotropic zeolite membranes with nanoscopic defects that create shortcuts perpendicular to the transmembrane direction (x). We have found that the dimensionless ratio $D_y/(k_d \Delta y)$ can be used to estimate whether the shortcuts contribute significantly to the overall flux. Here D_y is the diffusion coefficient for motion in the plane of the membrane, k_d is the rate of desorbing into defect voids, and Δy is the spacing between adjacent defects. For values of $D_y/(k_d \Delta y) \gg 1$, we find that shortcuts increase the flux by significant amounts. The magnitude of the flux is increased as the imperfection spacing Δy is decreased. For small values of Δy, permeation through shortcuts becomes sorption-limited so that decreasing Δy further does not increase the flux through a single shortcut. However, as Δy is decreased, the concentration of shortcuts increases, thereby increasing the total contribution of the shortcuts to the flux. We have found regimes where increasing Δy or decreasing D_y decreases the overall flux, showing that permeation can be diffusion-limited by motion perpendicular to the transmembrane direction.

Keywords: Diffusion; Gas and vapor permeation; Microporous membranes; Theory

1. Introduction

Recent progress in zeolite membrane synthesis has suggested new opportunities for demanding gas, vapor and liquid separations because of the crystalline, microporous structures offered by zeolites [1–26]. However, the same crystallinity also poses the most demanding challenge for the fabrication and use of these membranes, i.e. the presence of unavoidable grain boundaries between neighboring crystals in these polycrystalline films. Although permeation [27] and imaging [28] techniques have recently revealed such defects, there is very limited understanding of the relation between the membrane's microstructure and its separation performance. Several investigations have suggested the existence of non-zeolitic intercrystalline pathways in order to explain the permeation behavior of different gas/vapor mixtures through MFI zeolite membranes [22,29]. We recently noted the absence of transport models that can account for the interplay between zeolitic and non-zeolitic pathways through these membranes [30]; here we introduce such a mathematical model.

In a series of studies we reported the synthesis, microstructural characterization and separation performance of MFI membranes made by seeded growth [6,9,11,20,21,24]. The synthesis consists of making a colloidal suspension of zeolite nanocrystals that is

* Corresponding author. Tel.: +1-413-545-1240; fax: +1-413-545-4490.
E-mail address: auerbach@chem.umass.edu (S.M. Auerbach).

0376-7388/01/$ – see front matter
PII: S0376-7388(00)00641-4

used to deposit a seed layer on a substrate, followed by secondary grain growth of the deposited nanocrystals of the seed layer leading to a continuous film. Characterization by microscopy and X-ray diffraction indicates that film growth proceeds by direct growth of the seed particles, leading to continuous columnar films with single grains extending along the film thickness, and exhibiting a preferred out-of-plane orientation such that the crystals are oriented with their *c*-axis perpendicular to the substrate. With this preferred orientation the straight and zig-zag MFI channels are oriented parallel to the substrate, forcing intracrystalline transmembrane transport to follow the tortuous, higher resistance paths along the *c*-axis.

In this class of *c*-out-of-plane oriented MFI membranes, we detected the presence of straight and open grain boundaries extending along the film thickness nearly in parallel with the zeolite grains, using fluorescent confocal optical microscopy [28]. In order to understand the permeation behavior of this class of MFI membranes, we need to take into account the transport anisotropy in the membrane grains (faster transport parallel to the membrane surface and slower transport in the transmembrane direction) and the presence of non-zeolitic porosity at the grain boundaries extending along the membrane thickness. The development of the mathematical model introduced here is thus motivated by the microstructure of these membranes.

Below we investigate perhaps the simplest model of isothermal, single-component permeation through an imperfect zeolite membrane with constant-pressure boundary conditions. We achieve this by studying permeation through a Langmuirian lattice in two dimensions, which is in contact with reservoirs that serve as sources and sinks of adsorbates. Langmuirian models involve regular lattices of identical adsorption sites where transport occurs via activated jumps between adjacent sites [31–38]. Defining the transmembrane direction along the *x*-axis, and the "plane" of the membrane along the *y*-axis, the rates with which particles hop between adjacent adsorption sites are k_x and k_y, respectively. Single-component permeation fluxes through perfect, Langmuirian membranes are rigorously independent of the jump rate k_y [33]. In this article, we explore permeation through *imperfect* Langmuirian membranes, to determine whether certain defect structures can make permeation fluxes depend on variables controlling motion along the *y*-direction.

In previous studies, we have simulated detailed aspects of activated permeation through relatively thin ($L < 0.2\,\mu$m), defect-free membranes using open-system kinetic Monte Carlo methods [37,38]. However, for the present study we wish to explore more realistic membrane thicknesses, on the order of $L = 1\,\mu$m. Because permeation simulation times scale roughly with L^2, kinetic Monte Carlo becomes extremely time consuming when applied to these thicker membranes. Instead, we apply a finite difference formulation of the diffusion equation [35,37,38], which is known to reproduce the transport properties of single-component Langmuirian systems much more efficiently than with kinetic Monte Carlo. Below we find that with a moderate density of voids in the membrane, permeation fluxes can be strongly influenced by jumps perpendicular to the transmembrane direction. This suggests that an oriented zeolite membrane may not produce the expected transport anisotropy if there is a sufficient density of defects in the membrane.

The remainder of this paper is organized as follows: Section 2 introduces the details of our model membrane system, and describes the finite difference formulation used to calculate permeation fluxes. Section 3 presents results and discussion for both perfect and imperfect Langmuirian membranes, and in Section 4 we give concluding remarks.

2. The membrane system

Fig. 1 shows the membrane system we will discuss in this paper. The inflow reservoir is assumed to be large, so that the chemical potential of the permeating species remains constant at all times in the reservoir. Similarly, the chemical potential of the permeating component in the outflow reservoir is held constant. For simplicity we will assume that the concentration in the outflow reservoir is held at zero so that any permeating molecules that reach the outflow reservoir have zero probability of returning to the zeolite membrane.

The membrane has a number of imperfections or defects. On the inflow side there is a pore that is at the same chemical potential as the inflow reservoir. On the outflow side there is an "erop," which is a pore in reverse. The space enclosed by the erop is at

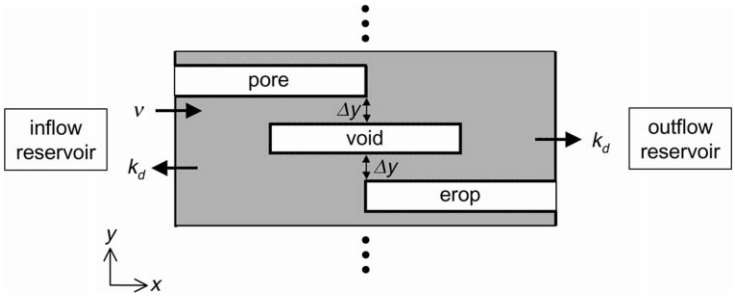

Fig. 1. Schematic representation of a Langmuirian zeolite membrane with nanoscopic defects. The membrane is of infinite extent in a plane perpendicular to the *x*-coordinate direction. The inflow reservoir is maintained at a constant pressure (defined by ν) and the outflow reservoir is maintained at vacuum ($\nu = 0$).

the same chemical potential as the outflow reservoir. As such, the pore is an extension of the inflow reservoir while the erop is an extension of the outflow reservoir. In addition, there is a void in the center of the membrane shown in Fig. 1. This void is a region devoid of zeolite that is accessible to the permeating molecules. At any point in time, the chemical potential throughout the void is spatially homogeneous. Thus, the void may be considered as an internal reservoir of permeating molecules. The assumption that the chemical potentials in the pore, void and erop are spatially homogeneous is equivalent to assuming that transport within these regions is much faster than intracrystalline transport in the zeolite. This is justified by the fact that gaseous diffusion is generally many orders of magnitude faster than diffusion in zeolites.

For comparison with Fig. 1, we show in Fig. 2(a) a top view SEM (scanning electron microscope) image of an MFI membrane, and in Fig. 2(b) we show the corresponding cross sectional view (from Ref. [28]). Furthermore, Fig. 3 shows a confocal microscopy image that reveals the presence of grain boundaries (also from [28]). The close correspondence between the present model and actual membrane microstructure is evident from comparing Figs. 1–3. Despite this correspondence, the purpose of this paper is *not* to suggest the manufacture of membranes with particular microstructures, but rather to explore the consequences of membrane microstructures that arise from modern synthetic techniques.

2.1. Langmuirian zeolites

In this paper, we investigate perhaps the simplest, realistic model for single-component permeation through zeolite membranes, the “Langmuirian”

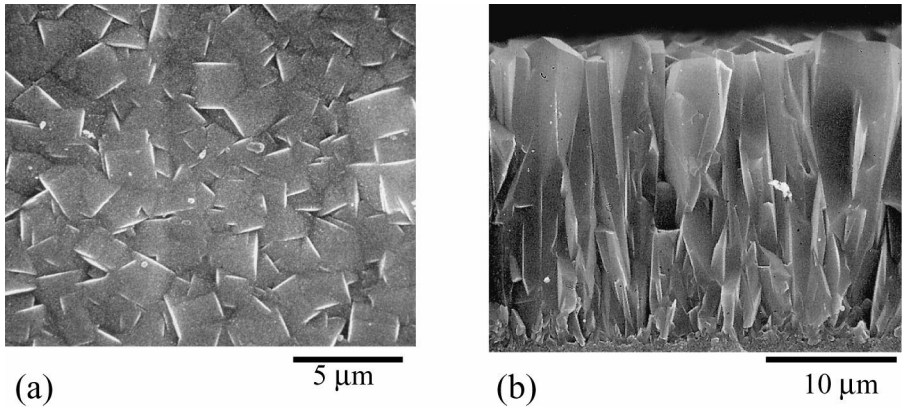

Fig. 2. SEM (scanning electron microscope) image of an MFI membrane; (a) top view; and (b) cross sectional view (from [28]).

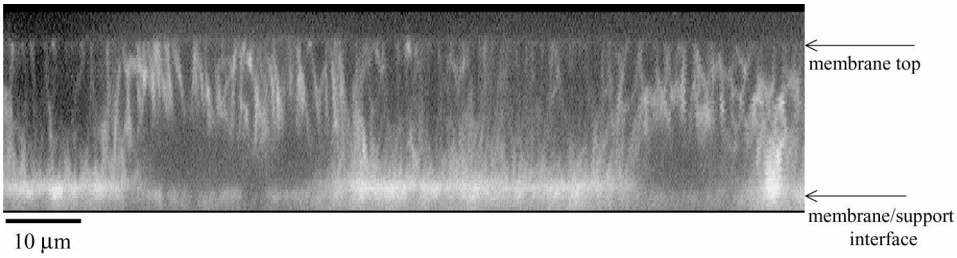

Fig. 3. Confocal microscopy image showing grain boundaries (from [28]). Correspondence between the present model and actual membrane microstructure is evident.

model. This model has been extensively investigated [31–38], and has been shown to quantitatively model adsorption and diffusion for many zeolite host–guest systems over a wide range of conditions. As described in more detail elsewhere [37], Langmuirian models involve regular lattices of identical adsorption sites where transport occurs via activated jumps between adjacent sites. In addition, such models ignore guest–guest interactions except for exclusion of multiple site-occupancy. Such models exhibit Langmuir adsorption isotherms, and give single-component transport diffusivities that are independent of loading. A typical example is cyclohexane in silicalite, where experimental results are consistent with the Langmuirian model up to a maximum loading of four molecules per unit cell [39]. Such behavior should be expected because silicalite channel intersections, where cyclohexane is adsorbed, are separated by a relatively large distance, so that the molecules in adjacent sites do not interact strongly.

Diffusion in Langmuirian systems proceeds by a sequence of thermally activated jumps, in which a sorbate molecule jumps from one site to a vacant nearest neighbor site, only after overcoming an energy barrier of E_x in the x-direction. Attempted jumps to occupied sites are unsuccessful because double occupancy of adsorption sites is forbidden. The rates with which a particle attempts to hop from one adsorption site to an adjacent site in the x- and y-directions, respectively, are given by

$$k_x = a_x \exp(-\beta E_x) \text{ and } k_y = a_y \exp(-\beta E_y), \quad (1)$$

where $\beta = 1/k_B T$, k_B is Boltzmann's constant, and E_x and E_y are the activation energies for jumping between two adjacent sites in the x- and y-directions, respectively. We define the anisotropy parameter, η, by the ratio

$$\eta = \frac{k_y}{k_x}, \quad (2)$$

of the attempted jump rates in the y- and x-directions. $\eta = 1$ corresponds to an isotropic lattice, $\eta > 1$ corresponds to a membrane where the jump rate in the transmembrane direction is slower, and $\eta < 1$ corresponds a membrane where diffusion is faster in the transmembrane direction. Single-component permeation fluxes through perfect, Langmuirian membranes are rigorously independent of the jump rate k_y. We explore the influence of diffusion anisotropy on permeation through *imperfect* Langmuirian membranes (see Fig. 1) by varying η over several orders of magnitude. For values of $\eta \neq 1$, η depends on temperature; we vary η by fixing E_x and varying E_y to give a desired value of η at a particular temperature, to be discussed further below.

The rate coefficient for desorption of a molecule from an edge site into any non-zeolitic region such as either of the reservoirs (including the pore and erop), or into the void, is given by

$$k_d = a_d \exp(-\beta E_d). \quad (3)$$

Hence, we assume that desorption from the lattice is a thermally activated process with an activation energy given by the heat of adsorption, as has been done previously [37,38].

For sites exposed to the inflow reservoir, at the left-hand edge of the membrane or at the edges of the pore, adsorption into the zeolite is controlled by an attempted insertion rate given by

$$\nu = a\, \rho_{gas} \sqrt{T}. \quad (4)$$

In using Eq. (4), we have assumed that the inflow reservoir is an ideal gas phase [37,38]. a is a prefactor determined by the surface topology of the zeolite and the mass of the molecule, ρ_{gas} is the gas phase density and T is the absolute temperature. Eq. (4) is also used for sites exposed to the void; however, in the void ρ_{gas} is not constant but rather is a free variable determined by the accumulation of permeating molecules in the void.

The processes governed by the rates k_x, k_y, k_{d}, and ν are assumed to be independent, Poisson processes with an instantaneous probability that is Markovian, i.e. the probability only depends on the current state of the system, and as such does not depend on the system's history. Throughout the paper, as well as in our earlier work [37,38], we use input parameters characteristic of cyclohexane in silicalite, motivated by the measurements of Magalhães et al. [39]; please see [37] for more details. Briefly, these parameters are $E_{\text{d}} = 17.5\,\text{kcal mol}^{-1}$ and $E_x = 11.5\,\text{kcal mol}^{-1}$. We generally expect that $k_{\text{d}} \ll k_x$; however, if k_{d} is too small the simulations may become intractable. To keep the simulations reported in [37] tractable, we studied the case where $k_{\text{d}} = k_x/100$, which corresponds to the temperature $T = 656\,\text{K}$ using the above activation energies measured by Magalhães et al. In the present study, we model membrane permeation at different temperatures and for different values of the anisotropy, η. Since in general η depends on temperature, we need to quote values of η at a reference temperature. Unless otherwise specified, we quote values of η at $T = 656\,\text{K}$, for consistency with our previous studies of membrane permeation. As such, we explore the effect of diffusion anisotropy by varying direction-dependent activation energies, and determining the temperature-dependent consequences of such variations.

A Langmuirian zeolite exposed to a fluid without external driving forces will have an adsorption isotherm of the form

$$\theta_{\text{eq}} = \frac{1}{1 + (k_{\text{d}}/\nu)}, \tag{5}$$

where θ_{eq} is the equilibrium occupancy. Eq. (5) can be derived by equating the rate of actual insertion, $\nu(1-\theta_{\text{eq}})$, and the rate of desorption, $k_{\text{d}}\theta_{\text{eq}}$, at equilibrium. Because our goal is a kinetic transport study, this kinetic form of the Langmuir isotherm is the most relevant. For an isothermal ideal gas, ν is proportional to the gas pressure, and the more usual form of the Langmuir isotherm is thus recovered

$$\theta_{\text{eq}} = \frac{1}{1 + (b/p)}, \tag{6}$$

giving occupancy as a function of the pressure, p. In this study, we compute the temperature dependence of permeation fluxes at constant pressure. The parameter ν is chosen at $T = 656\,\text{K}$ to give a target value of θ_{eq} at the inflow edge; ν is then scaled according to $\nu T^{1/2} = \text{constant}$, to keep the pressure fixed.

2.2. Finite difference formulation of diffusion

The theory of adsorption and diffusion in Langmuirian host–guest systems is well-developed [31,32,35,37] and is based on a finite difference formulation (FDF) of diffusion, which we briefly describe below. Because nodes in the finite difference formulation represent adsorption sites, the natural grid spacing in the FDF is the distance between adjacent sites. It is well-established that the FDF for a single component Langmuirian host–guest system gives the same numerical results as a large ensemble of kinetic Monte Carlo simulations [37]. Hence, in this work we will utilize the FDF to investigate the effect of a particular microstructure on permeation through anisotropic membranes.

We define the spatially and temporally varying occupancies of the permeating specie in the Langmuirian membrane as follows: $\theta_{x,y}(t)$ is the concentration of particles at time t at site (x,y), also known as the local site occupancy fraction at this point. This concentration should be considered as an ensemble average over large number of identical systems with identical boundary conditions. An alternate interpretation of $\theta_{x,y}(t)$ is that it represents the probability of finding a particle at adsorption site (x,y) at time t. In what follows, we will omit the explicit dependence on site position (x,y) and time t, i.e. $\theta_{x,y}(t) \to \theta$, unless clarity requires otherwise. We model transient behavior as a convenient method for approaching and numerically simulating steady states. Direct modeling of steady states is also possible; however, with the present pore-void-erop membrane microstructure, such modeling would require an inconvenient self-consistent approach, because the density of particles in the void is not known beforehand.

For diffusion in the interior of the lattice, we can write

$$\frac{\delta\theta_{x,y}}{\delta t} = \frac{D_x}{(\delta x)^2}(\theta_{x-1,y} - \theta_{x,y}) + \frac{D_x}{(\delta x)^2}(\theta_{x+1,y} - \theta_{x,y}) + \frac{D_y}{(\delta y)^2}(\theta_{x,y-1} - \theta_{x,y}) + \frac{D_y}{(\delta y)^2}(\theta_{x,y+1} - \theta_{x,y}), \quad (7)$$

for the bulk of the zeolite. If the site is an edge site then one of the four terms on the right-hand side of Eq. (7) should be replaced by the term

$$\frac{D_x}{(\delta x)^2}(\theta_{x-1,y} - \theta_{x,y}) \overset{\text{surface}}{\rightarrow} \nu(1 - \theta_{x,y}) - k_d\theta_{x,y}. \quad (8)$$

Note that the surface term does not include a length scale. This means that the grid point should correspond to an actual surface site. Although the finite difference grid can be mapped naturally onto the array of adsorption sites, it can also be mapped onto a grid with spacing larger than the distance between adsorption sites. This corresponds to solving the continuous differential equation for diffusion (Fick's second law) numerically on a grid, where the grid spacing is controlled by the spatial variation of density across the membrane. Using FDF grid spacings larger than site-to-site distances is appropriate when density variations are relatively small over such length scales. This approach can result in significant increases in the numerical efficiency of the algorithm.

Eq. (7) results in part from Fick's first law, $J = -D\nabla\theta$. In the alternative treatment of permeation, the Maxwell–Stefan formulation, the flux is given by

$$J = -L\nabla\mu, \quad (9)$$

where J is the particle flux, L is the Onsager coefficient and $\nabla\mu$ is the chemical potential gradient in a non-equilibrium system. The approach we take in this paper is entirely consistent with Eq. (9) [35,37], in the sense that the Fickian and Stefan–Maxwell approaches would produce the same fluxes given the same driving forces, where $\nabla\theta$ and $\nabla\mu$ are related through the adsorption isotherm.

When analyzing permeation through zeolite membranes, it is commonly assumed that there are no mass transfer resistances external to the membrane, and that permeation is determined solely by intra-membrane transport [40]. In this "diffusion-limited" regime, the chemical potentials at the edges of the membrane are assumed to be the same as in the reservoirs they are contacting. This assumption of local thermodynamic equilibrium at the edges of the membrane is valid for relatively thick membranes, where $k_dL \gg D_x$, where L is the membrane thickness and D_x is the transmembrane Fickian diffusivity. However, as we have previously shown, this approximation breaks down for relatively thin membranes [35,37,38]. In the present paper, we will demonstrate that a change in the microstructure of an otherwise large membrane may change the membrane from being diffusion-limited to sorption-limited.

3. Results and discussion

The FDF was used to calculate the flux through various membrane configurations. The initial condition was that the zeolite was filled with an equilibrium-adsorbed amount of the permeating specie. The time-dependent evolution of the concentration profiles were then generated using Eqs. (7) and (8). Steady states were identified when the influx from the inflow reservoir was the same to numerical accuracy as the flux into the outflow reservoir.

3.1. Perfect membrane

As a test of the finite difference code, we calculated the flux through a perfect membrane, i.e. one with no pores, voids or erops. For this perfect system, an analytical expression for the steady-state flux can be derived. At steady state there is a linear concentration gradient from the inflow side at $x = 1$ to the outflow side at $x = L$. By applying Fick's first law of diffusion, we find that the flux, J, is given by

$$J = -D_x\left[\frac{\theta_L - \theta_1}{L - 1}\right]. \quad (10)$$

For large values of L, $L - 1$ can be replaced by L. At the inflow edge, the flux is given by

$$J = \nu(1 - \theta_1) - k_d\theta_1. \quad (11)$$

The first term on the right-hand side is the rate of actual insertion of particles from the inflow reservoir into the sites in column $x = 1$. The second term on the

right-hand side is the rate of particle desorption from the sites in column 1 into the inflow reservoir. At the outflow edge, the flux is given by

$$J = k_d \theta_L, \tag{12}$$

as we have set the concentration in the outflow reservoir to be zero so that $\nu = 0$ at the outflow edge.

Eqs. (10)–(12) can be solved for the flux in terms of known quantities, yielding

$$J = \frac{\nu k_d D_x}{k_d L(\nu + k_d) + (\nu + 2k_d) D_x}. \tag{13}$$

If we substitute the kinetic form of the equilibrium adsorption isotherm, i.e. Eq. (5), into Eq. (13) we obtain

$$J = \frac{k_d \theta_{eq} D_x}{k_d L + (2 - \theta_{eq}) D_x}, \tag{14}$$

where θ_{eq} is the loading of the corresponding equilibrium system, with both reservoirs presenting insertion frequencies equal to ν. As discussed below for non-equilibrium systems, θ_{eq} is also the local concentration on the influx edge in the diffusion-limited regime.

Fig. 4 shows the flux, J, through a perfect membrane with $L = 1001$ sites as a function of temperature, for a constant pressure reservoir. We report flux in units of (number of permeating molecules) per (edge site) per (time unit), where the time unit is $1/(4k_x) = 2 \times 10^{-7}$ s, which is the mean residence time in an interior adsorption site of a perfect, isotropic lattice at $T = 656$ K. For the discussion below, we denote the temperature that gives the maximum flux, J_{max}, by the variable T_{max}. The FDF numerical method was found to give results identical to those predicted by Eq. (14). As shown in Fig. 4, the maximum flux arises because of the competition between the temperature dependencies of the diffusivity, D_x, and the equilibrium amount adsorbed, θ. It is the competition between these trends that accounts for the maximum in the flux, as can be seen by the close match between the FDF fluxes and those given by the product

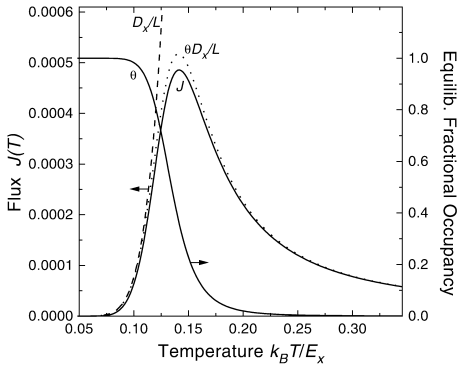

Fig. 4. Flux through a perfect membrane of thickness L as a function of temperature. The maximum in the flux, J (solid line), is caused by competition between the temperature dependencies of the equilibrium amount adsorbed, θ (solid line), and the diffusivity, D_x/L (dashed line). The dotted line, $\theta D_x/L$, indicates the flux in the thick membrane limit (see text).

$$J = \frac{\theta_{eq} D_x}{L}, \tag{15}$$

which is the limiting form of Eq. (14) when $k_d L \gg D_x$. Eq. (15) is the thick-membrane limit wherein permeation is diffusion-limited, and is also isomorphic to Fick's first law, $J = -D\nabla\theta$, where $D = D_x$ and $\nabla\theta = -\theta_{eq}/L$.

Bakker et al. have reported curves similar to those in Fig. 4 for permeation of lighter molecules through silicalite membranes [41]. A significant difference between our flux curve and that of Bakker et al. is that the latter gradually increases with temperature for temperatures well above T_{max}. In their analysis, there is an additional "gaseous" permeation term that is driven by the pressure drop across the membrane [41]. The "gaseous diffusivity" increases with temperature, while the pressure drop across the membrane remains constant by design, thereby producing increasing flux at high temperatures. Such an increase is inconsistent with the Langmuirian model discussed here as there is only a single mode of transport, namely, jump diffusion between well-defined adsorption sites. At high temperatures in our model, the adsorbed amount decreases more rapidly with temperature than the diffusivity D_x increases (see Eq. (15)).

For relatively thin Langmuirian membranes where $k_d L \ll D_x$, the flux is given by

$$J = \frac{k_d \theta_{eq}}{(2 - \theta_{eq})}. \tag{16}$$

This is the sorption-limited extreme where the concentration throughout the membrane is constant with the value

$$\theta_L = \frac{\theta_{eq}}{(2 - \theta_{eq})}. \tag{17}$$

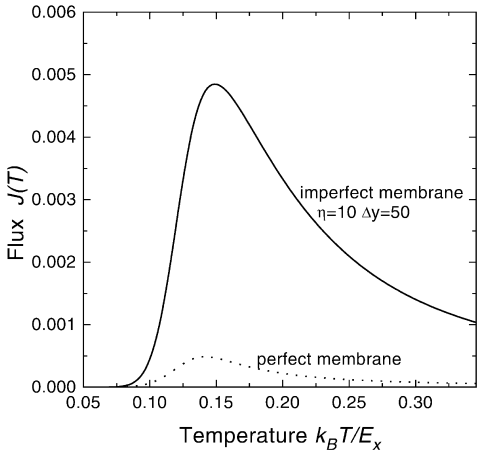

Fig. 5. Comparison of fluxes through an anisotropic imperfect membrane with nanoscopic defects, as shown in Fig. 1, and a perfect membrane as a function of temperature.

In this regime the intracrystalline chemical potential is constant throughout the membrane interior, and is intermediate between those of the inflow and outflow reservoirs. Note that the thickness of the membrane does not appear in Eq. (16), indicating that the flux is independent of membrane thickness in the sorption-limited extreme.

3.2. Imperfect membranes

Fig. 5 shows the flux through the membrane shown in Fig. 1. The membrane is $L = 1000$ sites thick, corresponding to a 1 μm thick silicalite membrane. The vertical distance between the void and the pore, and the void and the erop is $\Delta y = 50$ sites. The pore, void and erop are 500 sites wide and 50 sites high. Instead of applying the usual periodic boundary conditions to this membrane in the *y*-direction, we applied reflective boundary conditions, so that the *y*-component of the flux is zero across the top and bottom sites of the membrane shown in Fig. 1. These reflective boundary conditions, which are equivalent to impermeable grain boundaries, are implemented using impermeable sites at the top and bottom edge, and produce a membrane of infinite extent in the *y*-direction. The results in Fig. 5 were obtained with an anisotropy factor of $\eta = 10$ at $T = 656\,\mathrm{K}$ for the cyclohexane in silicalite system, by adjusting E_y as discussed above.

As can be seen from Fig. 5, the flux through the imperfect membrane has a similar functional form to that for the perfect membrane, but with a maximum flux that is about ten times larger. If molecules only travel in the *x*-direction, the effective membrane thickness would be about one-half that of a perfect membrane. This would account for about a two-fold increase in the flux; the additional increase in flux must therefore be produced by molecules taking shortcuts through the membrane as shown schematically in Fig. 6. In taking such shortcuts, the molecules pass through two thin zeolite sections of thickness Δy, with a combined thickness of about one-tenth that of the perfect membrane. Although we predict higher fluxes for this imperfect, anisotropic membrane, permselectivities obtained from this membrane may be lower than those for defect-free membranes, because the *effective* membrane thickness is much smaller than the actual thickness.

As discussed in Section 1, the goal of this study is to explore the influence of microstructural defects on

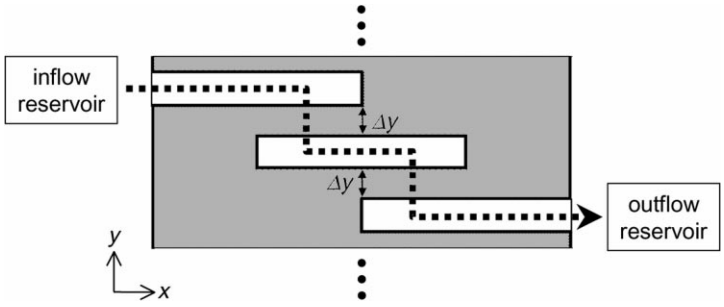

Fig. 6. Schematic representation of a shortcut through the anisotropic membrane of Fig. 1. In the shortcut, the diffusion in the *y*-direction is controlling.

permeation though anisotropic zeolite membranes. We wish to determine whether certain defect structures can make permeation fluxes depend on variables controlling motion along the *y*-direction, even though this is perpendicular to the transmembrane, *x*-direction. In particular, we are interested in correlating fluxes with the following variables: the diffusivity along the *y*-direction, $D_y = \eta D_x$; and Δy, the distance between adjacent defects. As discussed above for perfect membranes, permeation is diffusion-limited when $k_d L \gg D_x$ and is sorption-limited when $k_d L \ll D_x$. Now, for *imperfect* membranes, we want to know whether shortcut-dominated permeation may be diffusion-limited when $k_d \Delta y \gg D_y$ and sorption-limited when $k_d \Delta y \ll D_y$.

To explore how flux depends on $D_y = \eta D_x$, we varied the diffusion anisotropy η keeping E_x fixed as discussed above. Fig. 7 shows the peak flux, J_{max}, as a function of diffusion anisotropy for two values of the distance between defects, Δy. Because the diffusion anisotropy varies with temperature, we plot J_{max} against the value of η at the temperature T_{max}, corresponding to the maximum flux. At low values of the anisotropy, diffusion in the *y*-direction is slowed down dramatically and transport through the shortcut becomes negligible. As a result, the flux approaches a constant value for small η. When $\Delta y \ll L$, this constant flux is related to the average length of defects along the *x*-direction. For example, with defects that extend half the membrane thickness, as in Figs. 1 and 6, the asymptotic flux for small η will be roughly twice that for a perfect membrane, ca. $2 \times 0.0005 = 0.001$. The flux for small η decreases as Δy increases, approaching the perfect-membrane value of about 0.0005 as $\Delta y \to \infty$. This is because for fixed values of η and increasing Δy, the distance between imperfections becomes sufficiently large that the fraction of flux through the shortcut becomes minimal, so that flux approaches that for a perfect membrane.

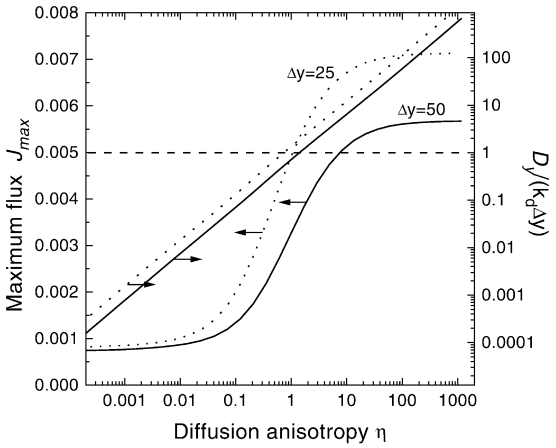

Fig. 7. Maximum flux as a function of diffusion anisotropy at the maximum flux temperature, $\eta(T_{max})$, for imperfect membranes with two different imperfection spacings $\Delta y = 50$ (solid lines) and $\Delta y = 25$ (dotted lines). Also shown is the dimensionless ratio, $D_y/(k_d \Delta y)$, which successfully predicts whether shortcuts contribute significantly to the overall flux.

Also shown in Fig. 7 is the dimensionless ratio, $D_y/(k_d \Delta y)$, which reflects whether permeation through the shortcut is diffusion- or sorption-limited. At high values of diffusion anisotropy, $D_y/(k_d \Delta y)$ becomes large and the shortcut flux approaches a sorption-limited value. In this regime, the magnitude of shortcut flux depends on Δy because the concentration of imperfections in the *y*-direction is controlled by Δy. For example, there is one shortcut per 300 sites when $\Delta y = 50$ and one shortcut per 225 sites when $\Delta y = 25$.

The dimensionless ratio $D_y/(k_d \Delta y)$ appears to be a good indicator for when shortcut flux is significant. For values of $D_y/(k_d \Delta y)$ much less than unity, the shortcut flux produces a negligible contribution to the overall flux. However, for large values the shortcut flux becomes significant. In this case, the overall flux will *not* exhibit the usual L^{-1} dependence expected for a perfect, diffusion-limited membrane. Indeed, in actual permeation measurements the flux often decreases with L to a plateau value and not to zero [21]; our calculations suggest that this plateau arises when shortcut flux through defects dominates normal flux.

For values of η between 0.1 and 1.0 using the parameters in our model, permeation flux correlates well with D_y, i.e. *transmembrane flux is strongly influenced by the rate of jumps along the y-direction*. As an example of the consequence of such a transport regime, consider *p*-xylene permeation through a *c*-oriented silicalite membrane [20,21,42]. Although such a membrane may be continuous in that it lacks pinholes, the membrane may have a sufficient density of voids to make transmembrane flux influenced by *p*-xylene motion down the *b*-axis, i.e. the straight channels. This is in contrast to transport diffusion

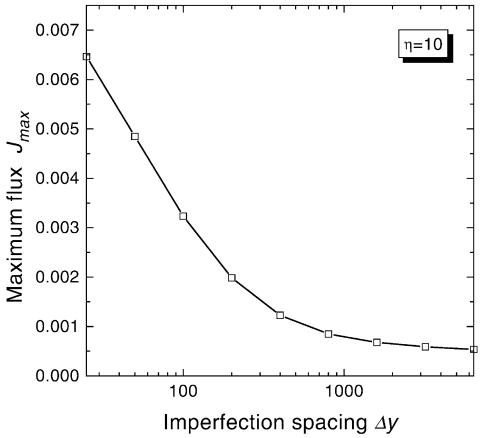

Fig. 8. Maximum flux as a function of imperfection spacing, for a diffusion anisotropy of $\eta = 10$. For small imperfection spacings the shortcut flux dominates; whereas, for larger imperfection spacings the flux approaches that of a perfect membrane.

through perfect Langmuirian membranes, for which permeation flux is rigorously independent of D_y. At values of $D_y/(k_d \Delta y)$ close to unity, the flux is approximately halfway between the limit of a perfect membrane and the limit where shortcut flux dominates.

Fig. 8 shows the variation of peak flux as a function of the spacing between imperfections, for a system where $\eta = 10$ at $T = 656\,\mathrm{K}$ for the cyclohexane in silicalite system discussed above. The first two points in Fig. 8 correspond to $\Delta y = 25$ and 50, respectively. As discussed above, the flux decreases as the concentration of imperfections decreases. As the spacing between imperfections increases, the flux decreases towards the perfect-membrane value of about 0.0005. The decrease of J_{max} with Δy shown in Fig. 8 provides another signature of the regime where permeation flux is diffusion-limited along the *y*-direction. This is analogous to the diffusion-limited case of a perfect membrane, where J_{max} decreases with membrane thickness *L*.

4. Conclusions

We have modeled permeation through anisotropic zeolite membranes with nanoscopic defects. Configurations of defects that create shortcuts perpendicular to the transmembrane direction have been investigated. We have shown that the addition of void-like defects can have a dramatic effect on the flux through the membrane, particularly if diffusion in the plane of the membrane is significantly faster than diffusion in the transmembrane direction. We have found that the dimensionless ratio $D_y/k_d \Delta y$ can be used to estimate whether the shortcuts contribute significantly to the overall flux. Here D_y is the diffusion coefficient for motion perpendicular to the transmembrane direction, k_d is the rate of desorbing into defect voids, and Δy is the spacing along *y* between adjacent defects. For values of $D_y/k_d \Delta y \gg 1$ we find that shortcuts increase the flux by significant amounts. The magnitude of the flux is increased as the imperfection spacing Δy is decreased. For small values of Δy, permeation through shortcuts becomes sorption-limited so that decreasing Δy further does not increase the flux through a single shortcut. However, as Δy is decreased, the concentration of shortcuts increases, thereby increasing the total contribution of the shortcuts to the flux. We have found regimes where increasing Δy or decreasing D_y decreases the overall flux, showing that permeation can be diffusion-limited by motion perpendicular to the transmembrane direction. In the context of *c*-out-of-plane oriented MFI membranes, this finding suggests that with the appropriate distribution of open grain boundaries even *c*-oriented membranes can behave like *b*- or *a*- oriented films.

Acknowledgements

S.M.A. thanks the National Science Foundation (CAREER, CTS-9734153) and the National Environmental Technology Institute for generous funding. M.T. acknowledges support from the National Science Foundation (CAREER, CTS-9612485) and the David and Lucile Packard Foundation for a Fellowship in Science and Engineering.

References

[1] E.R. Geus, H. van Bekkum, W.J.W. Bakker, J.A. Moulijn, Microporous Mater. 1 (1993) 131.
[2] Y. Yan, M. Tsapatsis, G.R. Gavalas, M.E. Davis, J. Chem. Soc., Chem. Commun. 2 (1995) 227.
[3] Y. Yan, M.E. Davis, G.R. Gavalas, Ind. Eng. Chem. Res. 34 (1995) 1652.
[4] Z.A.E.P. Vroon, K. Keizer, M.J. Gilde, H. Verweij, A.J. Burggraaf, J. Membr. Sci. 113 (1996) 293.

[5] H.H. Funke, M.G. Kovalchick, J.L. Falconer, R.D. Noble, Ind. Eng. Chem. Res. 35 (1996) 1575.
[6] M.C. Lovallo, M. Tsapatsis, AIChE J. 42 (1996) 3020.
[7] J. Coronas, J.L. Falconer, R.D. Noble, AIChE J. 43 (1997) 1797.
[8] J. Coronas, R.D. Noble, J.L. Falconer, Ind. Eng. Chem. Res. 37 (1998) 166.
[9] M.C. Lovallo, A. Gouzinis, M. Tsapatsis, AIChE J. 44 (1998) 1903.
[10] Z.A.E.P. Vroon, K. Keizer, A.J. Burggraaf, H. Verweij, J. Membr. Sci. 114 (1998) 65.
[11] G. Xomeritakis, A. Gouzinis, S. Nair, T. Okubo, M. He, R.M. Overney, M. Tsapatsis, Chem. Eng. Sci. 54 (1999) 3521.
[12] V.A. Tuan, J.L. Falconer, R.D. Noble, Ind. Eng. Chem. Res. 38 (1999) 3635.
[13] M. Kondo, M. Komori, H. Kita, K.-I. Okamoto, J. Membr. Sci. 133 (1997) 133.
[14] C.M. Braunbarth, L.C. Boudreau, M. Tsapatsis, J. Membr. Sci. 174 (2000) 31.
[15] C.D. Baertsch, H.H. Funke, J.L. Falconer, R.D. Noble, J. Phys. Chem. 100 (1996) 7676.
[16] A.J. Burggraaf, Z.A.E.P. Vroon, K. Keizer, H. Verweij, J. Membr. Sci. 144 (1998) 77.
[17] K. Keizer, A.J. Burggraaf, Z.A.E.P. Vroon, H. Verweij, J. Membr. Sci. 147 (1998) 159.
[18] K. Wegner, J. Dong, Y.S. Lin, J. Membr. Sci. 158 (1999) 17.
[19] H.W. Deckman, E.W. Corcoran, J.A. Mc Henry, W. Lai, L.R. Czarnetzki, W.E. Wales, US Patent 5,968,366 (1999).
[20] G. Xomeritakis, M. Tsapatsis, Chem. Mater. 11 (1999) 875.
[21] G. Xomeritakis, S. Nair, M. Tsapatsis, Microporous Mesoporous Mater. 38 (2000) 61.
[22] C.J. Gump, R.D. Noble, J.L. Falconer, Ind. Eng. Chem. Res. 38 (1999) 2775.
[23] M. Noack, P. Kolsch, J. Caro, M. Schneider, P. Toussaint, I. Sieber, Microporous Mesoporous Mater. 35 (2000) 253.
[24] A. Gouzinis, M. Tsapatsis, Chem. Mater. 10 (1998) 2497.
[25] A.J. Burggraaf, J. Membr. Sci. 155 (1999) 45.
[26] F. Kapteijn, J.M. van de Graaf, J.A. Moulijn, AIChE J. 46 (2000) 1096.
[27] J.C. Poshusta, R.D. Noble, J.L. Falconer, J. Membr. Sci. 160 (1999) 115.
[28] G. Bonilla, M. Tsapatsis, G Xomeritakis, D.G. Vlachos, J. Membr. Sci., in press.
[29] X. Lin, J.L. Falconer, R.D. Noble, Chem. Mater. 10 (1998) 3716.
[30] M. Tsapatsis, G. Xomeritakis, H.W. Hillhouse, S. Nair, V. Nikolakis, G. Bonilla, Z. Lai, Cattech 3 (2000) 148.
[31] J. Kärger, D.M. Ruthven, Diffusion in Zeolites and Other Microporous Solids, Wiley, New York, 1992.
[32] N.Y. Chen, T.F. Degnan Jr., C.M. Smith, Molecular Transport and Reaction in Zeolites, VCH Publishers, New York, 1994.
[33] R. Kutner, Phys. Lett. A 81 (1981) 239.
[34] D. Theodorou, J. Wei, J. Catal. 83 (1983) 205.
[35] P.H. Nelson, A.B. Kaiser, D.M. Bibby, J. Catal. 127 (1991) 101.
[36] P.H. Nelson, J. Wei, J. Catal. 136 (1992) 263.
[37] P.H. Nelson, S.M. Auerbach, Chem. Eng. J. 74 (1999) 43.
[38] P.H. Nelson, S.M. Auerbach, J. Chem. Phys. 110 (1999) 9235.
[39] F.D. Magalhães, R.L. Laurence, W.C. Conner, J. Phys. Chem. B 102 (1998) 2317.
[40] R. Krishna, L.J.P. van den Broeke, Chem. Eng. J. 57 (1995) 155.
[41] W.J.W. Bakker, L.J.P. van den Broeke, F. Kapteijn, J.A. Moulijn, AIChE J. 43 (1997) 2203.
[42] G. Xomeritakis, Z. Lai, M. Tsapatsis, Ind. Eng. Chem. Res., in press (2001).